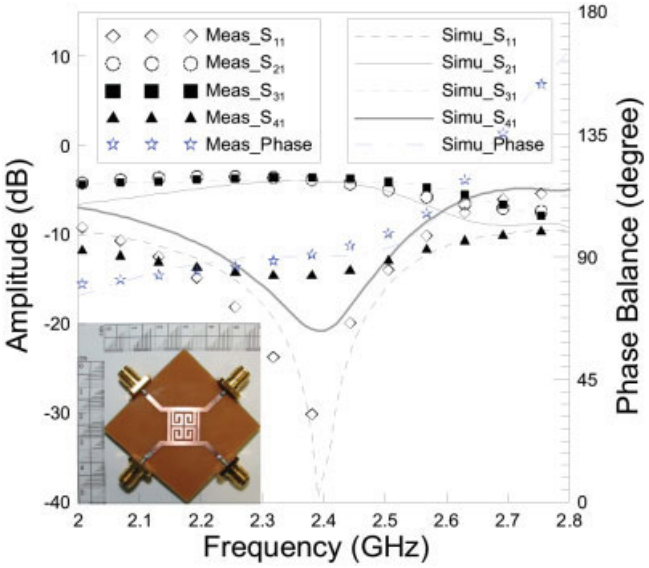

Figure 3 Frequency and phase responses of hi-impedance π-modeled microstrip branch-line coupler. [Color figure can be viewed in the online issue, which is available at www.interscience.wiley.com]

5°. Figure 4 also shows good agreements on the responses between the measurement and EM simulation.

4. CONCLUSION

A new approach to realize the miniaturize microstrip branch-line couplers has been proposed. Using the π-modeled approach, two types of planar branch-line couplers have been developed at the operating frequency of 2.4 GHz. The corresponding design equations have been described under ideal lossless conditions. The maximum achievable size reduction for the designed couplers is 62.92%. Moreover, these couplers can be fabricated using a standard PCB process, of which being easily applicable to the design of microwave or minimeter-wave integrated circuits.

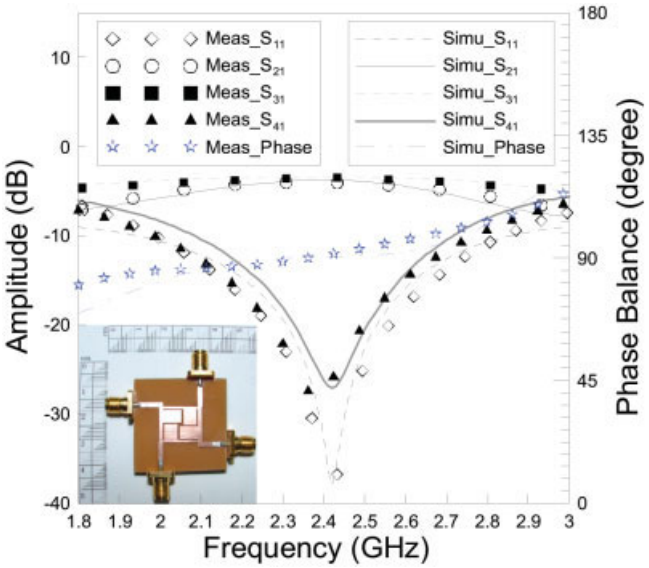

Figure 4 Frequency and phase responses of low-impedance π-modeled microstrip branch-line coupler. [Color figure can be viewed in the online issue, which is available at www.interscience.wiley.com]

ACKNOWLEDGMENTS

This work was supported in part by the National Science Council, Taiwan, under grant NSC 95–2221-E-194–029.

REFERENCES

1. J. Reed and G.J. Wheeler, A method of analysis of symmetrical four-port networks, IEEE Trans Microwave Theory Tech 4 (1956), 246–252.
2. J. Hongerheiden, M. Ciminera, and G. Jue, Improved planar spiral transformer theory applied to a miniature lumped element quadrature hybrid, IEEE Trans Microwave Theory Tech 45 (1997), 543–545.
3. H.R. Ahn, I.S. Chang, and S.W. Yun, Miniaturized 3-dB ring hybrid terminated by arbitrary impedances, IEEE Trans Microwave Theory Tech 42 (1994), 2216–2221.
4. M.C. Scardelletti, G.E. Ponchak, and T.M. Weller, Miniaturized Wilkinson power dividers utilizing capacitive loading, IEEE Microwave Wireless Compon Lett 12 (2002), 6–8.
5. T. Hirota, A. Minakaw, and M. Muraguchi, Reduced-size branch-line and rat-race hybrids for uniplanar MMIC's, IEEE Trans Microwave Theory Tech 38 (1990), 270–275.
6. K.O. Sun, S.J. Ho, C.C. Yen, and D. van der Weide, A compact branch-line coupler using discontinuous microstrip lines, IEEE Microwave Wireless Compon Lett 15 (2005), 519–520.

APODIZATION OF FIBER BRAGG GRATINGS BY USING ARC DISCHARGES

R. Romero,[1] G. Rego,[1,2] and P. V. S. Marques[1,3]
[1] UOSE, INESC-Porto, R. Campo Alegre 687, 4169-007 Porto, Portugal; Corresponding author: rromero@multiwavephotonics.com
[2] Escola Superior de Tecnologia e Gestão-IPVC, 4900-348 Viana do Castelo, Portugal
[3] FCUP, R. Campo Alegre 687, 4169-007 Porto, Portugal

Received 5 July 2007

ABSTRACT: *The electric arc technique is used to apodize fiber Bragg gratings (FBGs). Arc discharges applied to the ends of the grating produce a smoothing of the refractive-index modulation profile reducing the sidelobes of the reflection spectrum at longer wavelengths. A sidelobe reduction of 17 dB was obtained.* © 2007 Wiley Periodicals, Inc. Microwave Opt Technol Lett 50: 316–319, 2008; Published online in Wiley InterScience (www.interscience.wiley.com). DOI 10.1002/mop.23056

Key words: *fiber Bragg gratings; apodization; electric arc discharges*

1. INTRODUCTION

Fiber Bragg gratings (FBGs) represent one of the most significant developments in the field of optical fiber technology, due to their flexibility and unique filtering performance. In optical telecommunication applications, FBGs are recognized as key components in dense wavelength division multiplexing because of their low-insertion loss, high-wavelength selectivity, low-polarization dependent loss, and low-polarization modal dispersion.

In a Bragg grating with a uniform modulation of the refractive index, the main peak of the reflection spectrum is accompanied by series of sidelobes at adjacent wavelengths, because of the abrupt index change produced in the FBG fabrication between the average refractive index of the modulation profile and the initial refractive index of the fiber's core. In the case of DWDM applications, the reflection spectrum of the FBGs has to fulfill the required specifications that will necessarily lead to sidelobe reduc-

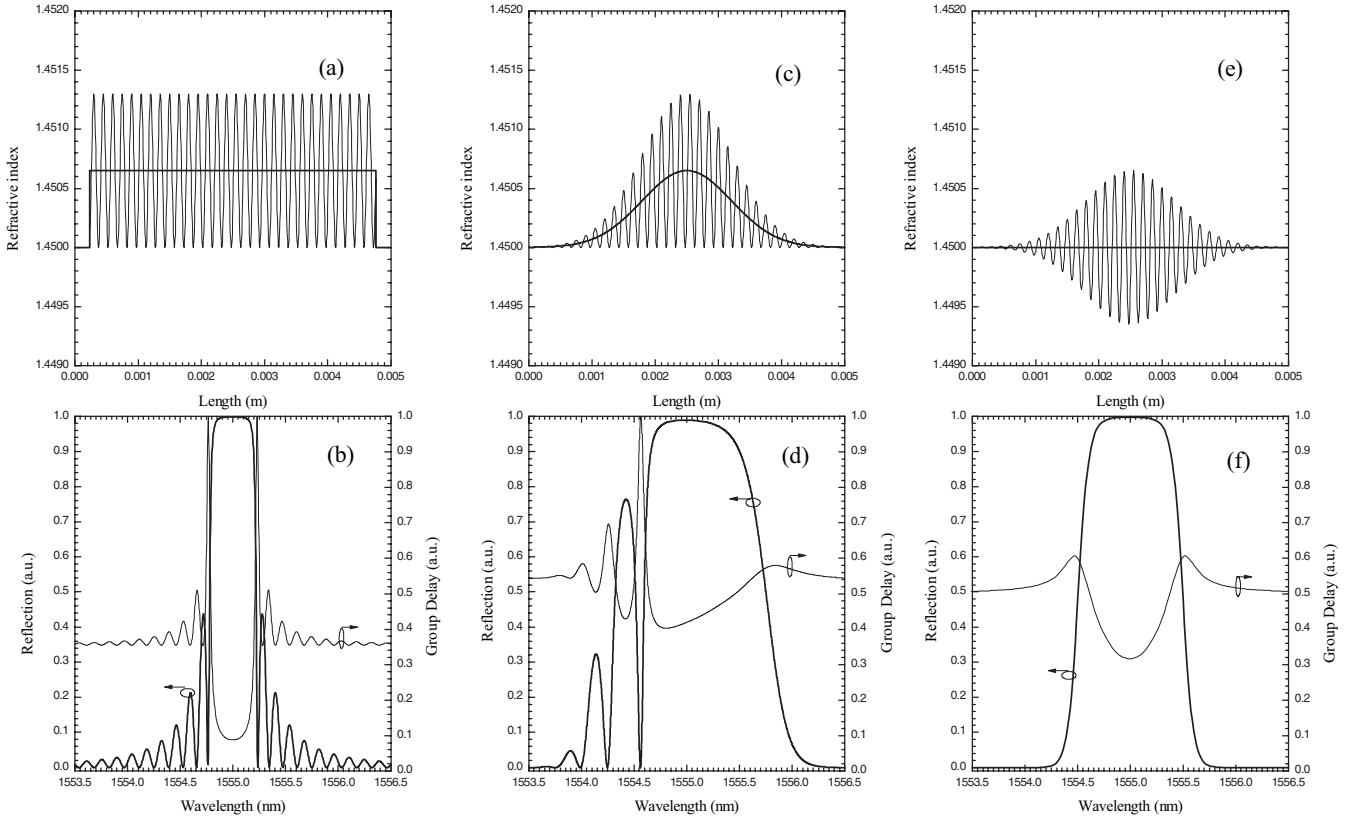

Figure 1 Uniform, nonuniform Gaussian and uniform Gaussian modulation amplitude profile of the refractive index (top) and the reflection spectra and group delay responses (bottom) calculated using the transfer-matrix method

tion to decrease crosstalk and increase isolation levels between adjacent channels. This sidelobe suppression comprises the tailoring of the modulation of the refractive index along the grating length and is called apodization.

Several methods have been used to apodize FBGs, namely, a phase mask with variable diffraction efficiency [1], automatic pure apodization through a phase mask [2], stretching the fiber [3], and UV-pulse interferometry [4]. In this article, the electric arc technique, which has been exploited in the fabrication of long period gratings [5], will be used to perform symmetric apodization of a uniform FBG.

2. THEORETICAL SIMULATIONS

As it was explain in the introduction, the well-known spectral response of a uniform FBG is not desirable in some optical communications applications due to the presence of the sidelobes, which are caused by the step produced in the average refractive index.

The refractive-index modulation profile of a FBG in the core of the fiber can be written in a general form as follows:

$$n(x) = n_0 + \Delta n = n_0 + \delta n\left[1 + \cos\left(\frac{2\pi x}{\Lambda}\right)\right], \qquad (1)$$

where n_0 is the refractive index of the core of the fiber, δn is the amplitude of the induced refractive-index modulation, and Λ is the spatial period of the modulation. Therefore, the total average refractive index in the FBG region can be easily written as

$$n_{av} = n_0 + \delta n. \qquad (2)$$

To apodize a FBG, this average refractive index should remain constant or it should have a smooth transition between the index of the core of the fiber and the average index in the grating region. However, the apodization of a FBG not only gives a reduction of the sidelobes but also changes its dispersion characteristics. Figure 1 shows the average and modulation of the refractive index of a uniform fiber Bragg [Fig. 1(a)] and two types of apodized FBGs [Figs. 1(c) and 1(e)]. This figure also shows numerical simulations of the reflection spectra and delays for these modulation refractive-index profiles. As it can be seen, the undesired sidelobes are present in the reflection spectrum of a uniform FBG [Fig. 1(b)], while the apodized FBGs show a reduction of the sidelobes [Figs. 1(d) and 1(f)]. The first apodization is a nonuniform Gaussian apodization [Fig. 1(d)] and consists on smoothing the step profile at the edges of a uniform FBG. This type of apodization causes a Fabry Perot cavity between the edges of the grating producing resonances at shorter wavelengths [6]. The second apodization is a uniform Gaussian apodization [Fig. 1(f)], in which the average refractive index of the FBG remains constant while the refractive-index modulation amplitude changes gradually. On the other hand, the apodization process of a FBG also changes dramatically the group delay characteristics of the FBGs reducing the delay ripples at the edges of the spectrum, as the bottom figures show.

To achieve a good apodization of a FBG, it is necessary to modify and measure the amplitude of the refractive-index modulation profile. This amplitude is related to the coupling coefficient through the expression [7]

$$\kappa = \frac{\pi \delta n \eta}{\lambda}, \qquad (3)$$

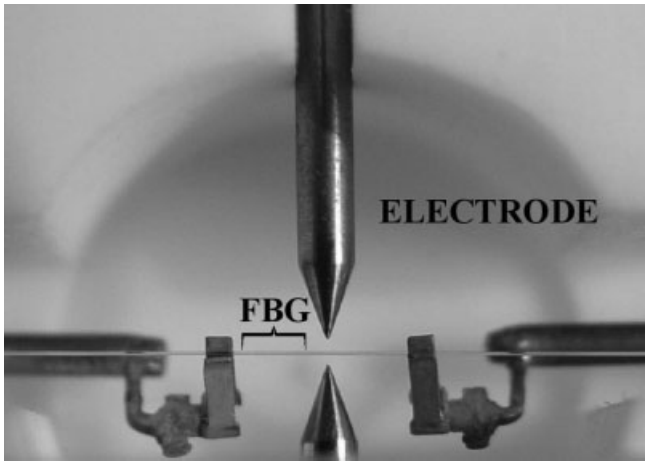

Figure 2 Photograph showing in detail the main part of the apodization setup

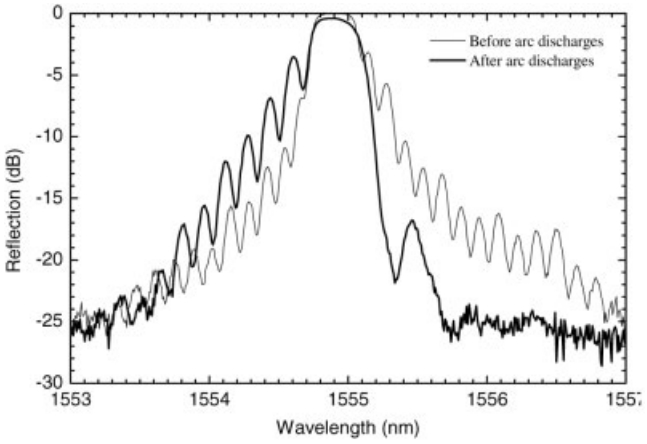

Figure 3 Reflection spectra versus wavelength. Initial FBG (solid line) and FBG with 35 discharges on both sides (bold solid line)

in which η is the fraction of the fiber mode power contained within the fiber core boundaries, and λ is the propagating wavelength in the FBG. The importance of the coupling coefficient is that it can be experimentally measured using optical frequency domain reflectometry [8] given thus information about the amplitude of the induced refractive-index modulation, δn. In forthcoming sections, the coupling coefficient will be measured to demonstrate nonuniform symmetric apodization of a uniform FBG using electric arc discharges.

3. FABRICATION

To demonstrate the apodization method, a uniform 5-mm long FBG centered at $\lambda_B = 1555$ nm and with a bandwidth (FWHM) of 0.3 nm was photoimprinted using a diffractive phase mask illuminated with a KrF excimer laser operating at 248 nm. The length of the FBG was chosen to be possible to measure the sidelobes in the optical spectrum analyzer (OSA) at its maximum resolution of 0.08 nm.

Figure 2 shows a close view of the FBG apodization setup. The fiber, placed on a motorized translation stage with a resolution of 0.1 μm, was longitudinally moved along its axis in such a way that the grating was moved toward the heating zone in steps of 200 μm. On each step, an electric arc discharge was produced with a current less than 9 mA during 0.5 s. After the grating have sensed the heat from the arc discharge for the first time, the steps were decreased to 50 μm and the time duration, t, was increased exponentially from 0.5 to 2.5 s as the grating was approaching the arc discharge region; 35 electric arc discharges on each side of the grating were needed to achieve the apodized grating as shown in Figure 3. The fiber movement and the arc discharges were synchronized by a personal computer. The whole process was monitored in real time using a broadband optical source and an OSA to obtain the best reflection spectrum for the apodization profile.

4. RESULTS AND DISCUSSION

The reflection spectrum of the grating after the apodization process (see Fig. 3) shows that the longer wavelength sidelobes were reduced due to the smoothing of the refractive-index modulation profile, as caused by the high temperature annealing during the arc discharges. The shorter wavelength resonances became more evident as a result of the average refractive-index change that produces cavity effects at those wavelengths [6, 9]. The spectrum also shows a slight decrease of the peak reflectivity as expected because the refractive-index modulation step profile was partially erased due to the high temperature applied by the electric arc discharges. The delay measurement [10], shown in Figure 4, presents the same behavior as a nonuniform apodized grating, when compared with Figure 1(d), confirming that the grating has been apodized and also shows cavity effects at shorter wavelengths.

To have a quantitative measurement of the variation of the amplitude of the modulation refractive-index profile, the optical frequency domain interferometry technique was used for the reconstruction of the spatial distribution of the coupling coefficient [8] along the grating region. Figure 5 shows a comparison between the coupling coefficients of two FBGs of the same length. One is a uniform FBG and the other is the nonuniform apodized FBG using electric arc discharges. For the uniform FBG, the coupling coefficient has a step profile while for the apodized FBG the profile is smoother at the edges of the grating region, as it was expected.

These results enable one to conclude that a nonuniform average refractive-index longitudinal distribution was obtained after the apodization process instead of the uniform FBG, as it was already predicted in previous theoretical sections. Better results are expected if a preconditioning photosensitivity response and effective index profile are accomplished by exposing the fiber to the electric arc before the grating photoinscription in the same region, achieving a uniform apodization as shown in Figures 1(e) and 1(f).

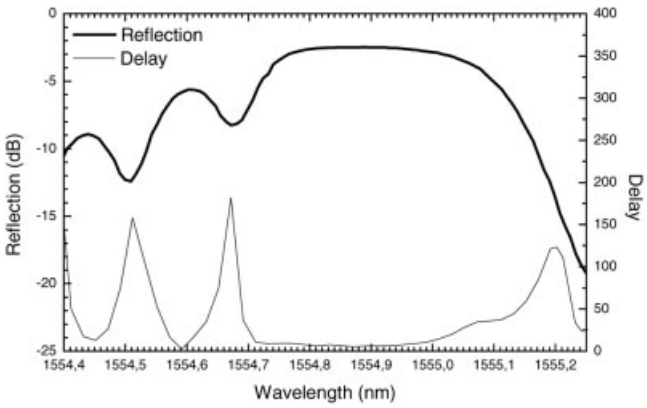

Figure 4 Reflection spectra (solid line) and group delay (dotted line) versus wavelength for a nonuniform apodized fiber Bragg grating

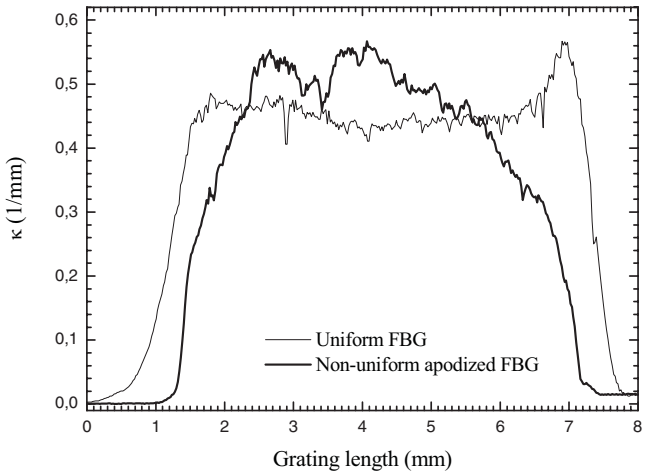

Figure 5 Reconstructed coupling coefficient versus position of a uniform (line) and nonuniform apodized (solid line) fiber Bragg grating

5. CONCLUSIONS

A FBG was apodized using the simple, reproducible, and fully automated electric arc discharge technique. The improvement of this apodization technique, which may be applied to any type of FBG, requires the definition of a preconditioning refractive index and/or photosensitivity response profile using also electric arc discharges.

ACKNOWLEGMENTS

We thank Sven Kieckbusch, from Technical University Hamburg Harburg (Hamburg Germany) for providing us the measurements of the reconstructed coupling coefficient used in this work.

REFERENCES

1. J. Albert, K.O. Hill, B. Malo, S. Thériault, F. Bilodeau, D.C. Johnson, and L.E. Erickson, Apodisation of the spectral response of fibre Bragg gratings using a phase mask with variable diffraction efficiency, Electron Lett 31 (1995), 222-223.
2. J. Albert, K.O. Hill, D.C. Johnson, F. Bilodeau, and M. Rooks, Moiré phase masks for automatic pure apodisation of fibre Bragg gratings, Electron Lett 32 (1996), 2260-2261.
3. R. Kashyap, A. Swanton, and D.J. Armes, Simple technique for apodising chirped and unchirped fibre Bragg gratings, Electron Lett 32 (1996), 1226-1228.
4. P.Y. Cortes, F. Ouellette, and S. LaRochelle, Intrinsic apodisation of Bragg gratings written using UV-pulse interferometry, Electron Lett 34 (1998), 396-398.
5. G. Rego, P.V.S. Marques, H.M. Salgado, and J.L. Santos, Arc-induced long-period gratings, Fiber Integr Opt 24 (2005), 245-259.
6. T. Erdogan, Fiber grating spectra, J Lightwave Technol 15 (1997), 1277-1294.
7. R. Kashyap, Fiber Bragg gratings, Academic Press, San Diego, CA, 1999.
8. S. Kieckbusch, C. Knothe, and E. Brinkmeyer, Fast and accurate characterization of fiber Bragg gratings with high spatial and spectral resolution, Opt Fiber Sensor (2003), 379-381.
9. V. Mizrahi and J.E. Sipe, Optical properties of photosensitive fiber phase gratings, J Lightwave Technol 11 (1993), 1513-1517.
10. C. Caspar, H.-M. Foisel, C.V. Helmolt, B. Strebel, and Y. Sugaya, Comparison of the cascadability performance of different types of commercially available wavelength (de)multiplexers, Proc. ECOC'97, 1997, pp. 91-94.

AN ANALYSIS OF SUBSTRATE EFFECTS ON TRANSMISSION-LINES FOR MILLIMETER-WAVE CMOS RFIC APPLICATIONS

Jin-Fa Chang,[1] Yo-Sheng Lin,[1] Chi-Chen Chen,[1] Chang-Zhi Chen,[1] Pen-Li Huang,[2,3] Tao Wang,[2,3] and Shey-Shi Lu[2,3]

[1] Department of Electrical Engineering, National Chi Nan University, Puli, Taiwan; Corresponding author: stephenlin@ncnu.edu.tw
[2] Graduate Institute of Electronics Engineering, National Taiwan University, Taipei, Taiwan
[3] Department of Electrical Engineering, National Taiwan University, Taipei, Taiwan

Received 5 July 2007

ABSTRACT: *A set of transmission lines (TLs) for millimeter-wave (MMW) CMOS RFIC applications was implemented in a standard 0.18 μm CMOS technology and then postprocessed by CMOS-compatible inductively-coupled plasma (ICP) etching, which removed the silicon underneath the TLs completely. TL parameters such as characteristic impedance Z_C, attenuation constant α, phase constant β, effective permittivity ε_{eff}, minimum noise figure (NF_{min}), parallel capacitance/conductance C/G, and series inductance/resistance L/R, as a function of frequency were extracted. It was found that α, ε_{eff}, NF_{min}, C, and G were greatly improved after silicon removal. The state-of-the-art performances of the on-chip TLs-on-air suggest that they are very suitable for application to realize ultralow-noise MMW CMOS RFICs. Besides, the CMOS-compatible backside ICP etching technique is very promising for MMW system-on-a-chip applications.* © 2007 Wiley Periodicals, Inc. Microwave Opt Technol Lett 50: 319–324, 2008; Published online in Wiley InterScience (www.interscience.wiley.com). DOI 10.1002/mop.23055

Key words: *substrate effects; transmission-line; millimeter-wave; low noise; CMOS; RFIC*

1. INTRODUCTION

In the design of millimeter-wave (MMW) low-noise-amplifiers (LNAs) for single-chip receiver front-end applications [1–3], the minimum noise figure (NF_{min}) of the transmission line (TL) used for interconnection at the input port of the LNAs is crucial for the overall NF performance of the LNAs. This is because the total NF (in dB) of an LNA is usually equal to the NF_{min} (or the inverse of maximum available power gain $1/GA_{max}$) of the input passive network, which normally includes a short piece of TL and an inductor, connected to the input transistor plus the NF of the other part of the LNA. The NF_{min} is obtained because the impedance match at both input and output ports of the input passive network is usually achieved simultaneously in the design, since the input impedance match and noise match of CMOS LNAs usually can be optimized simultaneously [4].

The NF_{min} performance of an RF passive device is limited by the loss in the conductive silicon substrate. Various methods have been proposed to reduce the substrate loss of RF passive devices, such as (wet etching based) front-side and backside micromachining [5–9], porous silicon [10, 11], proton implantation [12], and substrate transfer [13], etc. However, most of the proposed methods are inherently nonstandard CMOS processing steps. Fortunately, this problem can be improved to a large extent by our CMOS-compatible backside inductively-coupled-plasma (ICP) deep trench technology [14]. In this work, a set of TLs was implemented in a 0.18 μm CMOS technology and then postprocessed by ICP etching, which removed the silicon underneath the TLs to study the substrate effects on them. In addition to NF_{min},